# $Nd^{3+} \rightarrow Yb^{3+}$ resonant energy transfer in the ferroelectric $Sr_{0.6}Ba_{0.4}Nb_2O_6$ laser crystal

U. Caldiño,* D. Jaque, E. Martín-Rodríguez, M. O. Ramírez, and J. García Solé
*Departamento de Física de Materiales, Universidad Autónoma de Madrid, Cantoblanco, 28049 Madrid, Spain*

A. Speghini and M. Bettinelli
*Dipartimento Scientifico e Tecnologico, Università di Verona and INSTM, UdR Verona, Strada Le Grazie 15, I-37314 Verona, Italy*
(Received 12 July 2007; published 21 February 2008)

Resonant (nonphonon-assisted) $Nd^{3+} \rightarrow Yb^{3+}$ energy transfer has been observed in $Nd^{3+}$ and $Yb^{3+}$ codoped $Sr_{0.6}Ba_{0.4}(NbO_3)_2$ crystals. The $Nd^{3+} \rightarrow Yb^{3+}$ energy transfer in this system has been compared to those taking place in other $Nd^{3+}$-$Yb^{3+}$ codoped hosts, for which, in most of cases, the transfer is only possible by assistance of phonons. The resonant nature is explained as a result of both the very broad optical bands of $Nd^{3+}$ and $Yb^{3+}$ ions in $Sr_{0.6}Ba_{0.4}(NbO_3)_2$ and the short energy gap (636 $cm^{-1}$) between the $^4F_{3/2}$ ($Nd^{3+}$) and $^2F_{5/2}$ ($Yb^{3+}$) excited states. Spectroscopic data revealed that the energy transfer occurs via a nonradiative process and is dominated by an electric dipole-dipole interaction. The most relevant spectroscopic properties of the $Nd^{3+} \rightarrow Yb^{3+}$ energy transfer have been systematically investigated as a function of $Yb^{3+}$ ion concentration. The energy transfer efficiency increases linearly with the $Yb^{3+}$ ion concentration so that about a 50% is attained for a 10 at. % of ion acceptor concentration.

DOI: 10.1103/PhysRevB.77.075121 PACS number(s): 42.55.Rz, 42.62.Fi, 42.70.Hj, 42.70.Mp

## I. INTRODUCTION

There is an increasing interest in trivalent rare earth ion-doped nonlinear host crystals, since they emerge as promising materials for tunable and pulsed coherent light generation in the visible region. Of particular relevance is the case of $Yb^{3+}$ ion-doped nonlinear crystals, which have interest as potential solid-state laser materials emitting coherent radiation in the green by self-frequency doubling of its fundamental infrared laser line (around 1 $\mu$m).[1] The $Yb^{3+}$ ion has a unique pump channel, which avoids some problems such as upconversion, pump induced thermal loading, cross relaxation, and excited-state absorption. Moreover, the longer lifetime of $Yb^{3+}$ ions, compared to many other luminescent trivalent rare earth ions, allows for larger energy-storage efficiency. Nevertheless, because of the existence of only one excited state, optical excitation of $Yb^{3+}$ ions up to its metastable state can be only achieved within a reduced spectral range determined by the spectral extension of the $^2F_{7/2} \rightarrow {}^2F_{5/2}$ absorption band (located at around 980 nm). This is in contrast to the case of $Nd^{3+}$ doped lasers, in which the large number of excited states makes possible the use of a great variety of wavelengths for optical population of the metastable state. The existence of several pump channels (i.e., the possibility of using different pump wavelengths) is of special importance in nonlinear solid-state lasers, since the frequency mixing processes involving pump and laser radiations have been demonstrated to allow for tunable laser light generation in the blue.[2] Therefore, it is expected that the combination of the good properties of $Yb^{3+}$ and $Nd^{3+}$ ions could lead to an efficient $Yb^{3+}$ laser oscillation under $Nd^{3+}$ pumping via energy transfer (as it has been already demonstrated by Petit *et al.*[3]), giving place to a variety of intracavity frequency mixing processes for multifrequency generation and also allowing for optical pumping at different wavelengths.

Strontium barium niobate $Sr_xBa_{1-x}Nb_2O_6$ (SBN) crystal is a very interesting optical material due to its excellent piezoelectric, pyroelectric, electro-optic, and nonlinear coefficients. Its high electro-optic coefficients[4] make this crystal suitable for applications in optical data storage, optical computing, and switching. Its high nonlinear coefficients make this crystal as an excellent (self- or external-) frequency converter.[2,5]

According to these perspectives, we have systematically investigated the spectroscopic properties of the $Nd^{3+} \rightarrow Yb^{3+}$ energy transfer in congruent ($x=0.6$) SBN crystals in order to estimate the energy-transfer efficiency as well as to understand the mechanisms responsible for that transfer. Moreover, this SBN:Nd, Yb doubly doped system is particularly interesting because the absorption cross section of a number of $Nd^{3+}$-absorption bands is several times higher than those corresponding to the $Yb^{3+}$-absorption bands. This should lead to a final increase in the absorption efficiency of the whole laser system. Thus, it is expected that the present study will contribute to assess the performance of a possible multifunction optical material from $SBN:Nd^{3+}:Yb^{3+}$, with the possibility of short pulse and tunable coherent light generation in the blue-green spectral region.

## II. EXPERIMENT

$Sr_{0.6}Ba_{0.4}Nb_2O_6$ (SBN60) crystals doped with a fixed nominal concentration of $Nd^{3+}$ (1 at. % in the melt relative to $Nb^{5+}$) and variable nominal concentrations (1, 2, 5, 7, and 10 at. % in the melt relative to $Nb^{5+}$) of $Yb^{3+}$ ions were grown. We used a high temperature solution growth technique in fluxes consisting of mixtures of barium and strontium tetraborates,[6] containing suitable amounts of high purity (99.99%) $Nb_2O_5$, $Nd_2O_3$, and/or $Yb_2O_3$. Hereafter, the crystals studied SBN60:Nd (1 at. %), SBN60:Nd (1 at. %):Yb (1 at. %), SBN60:Nd (1 at. %):Yb (2 at. %), SBN60:Nd (1 at. %):Yb (5 at. %), SBN60:Yb (5 at. %), SBN60:Nd (1 at. %):Yb (7 at. %), and SBN60:Nd (1 at. %):Yb

 

(10 at. %) will be referred as Nd1, Nd1Yb1, Nd1Yb2, Nd1Yb5, Yb5, Nd1Yb7, and Nd1Yb10, respectively.

Continuous wave emission spectra were recorded by exciting with a cw Ti-sapphire laser tunable from 800 to 980 nm. The emitted light was focused onto a SPEX 500 M monochromator and then detected by a calibrated germanium detector. An EG&G lock-in amplifier was used to improve the signal to noise ratio. The excitation intensity was varied by changing the Ti-sapphire laser power.

Fluorescence decay-time measurements were made by exciting with an optical parametric oscillator (Quanta Ray), which provides 10 ns pulses with an average energy of 2 mJ and then detected by means of an AsGaIn cooled photomultiplier. Decay-time data were processed by a Le Croy model LT 372 digitizing oscilloscope. All measurements were performed at room temperature.

## III. STRONTIUM BARIUM NIOBATE STRUCTURE: LOCATION OF $Nd^{3+}$ AND $Yb^{3+}$ IONS

The SBN crystal has a tungsten bronze-type tetragonal structure with a $P4bm$ space group.[7] Its general formula is $(A1)_4(A2)_2(B1)_2(B2)_8O_{30}$. The Al sites (with $C_4$ symmetry) are partially occupied by $Sr^{2+}$ ions, up to 82.2% for $x=0.75$.[7] The A2 sites (with $C_s$ symmetry) are partially occupied in a disordered way by $Sr^{2+}$ and $Ba^{2+}$ host cations, up to 50.3% and 34.4%, respectively, for $x=0.75$.[7] The two distorted octahedral sites, B1 ($C_{2v}$ symmetry) and B2 ($C_1$ symmetry), are completely filled by $Nb^{5+}$ cations and have sixfold coordination.[7] There is also another interstitial empty site, the so-called C site,[7] with ninefold coordination and restricted to small-size impurities. On the other hand, oxygen vacancies are randomly distributed among the different oxygen sites, giving place to an additional disorder on the anionic oxygen sublattice. This large disorder results in strongly inhomogeneously broadened optical lines for the rare earth ions.[8] In SBN crystals, $Nd^{3+}$ ions very likely occupy A2 sites,[8] whereas $Yb^{3+}$ ions are distributed among the four different cationic lattice sites (A1, A2, B1, and B2).[9]

## IV. RESULTS AND DISCUSSION

The experimental results are organized as follows. First, we present absorption and luminescence results obtained for SBN60:$Nd^{3+}$ and SBN60:$Yb^{3+}$ singly doped crystals in order to discuss the suitability for $Nd^{3+} \rightarrow Yb^{3+}$ resonant energy transfer in the doubly doped SBN60:$Nd^{3+}$:$Yb^{3+}$ crystals. Then, we perform an analysis of luminescence decay-time data in order to determine the multipolar nature of the $Nd^{3+} \rightarrow Yb^{3+}$ energy transfer and the energy-transfer microparameter. Next, we investigate the effect of increasing the $Yb^{3+}$ (acceptor) concentration on the energy-transfer efficiency. Finally, we investigate the possibility of $Nd^{3+} \leftarrow Yb^{3+}$ back transfer processes for different excitation intensities, as it could lead to a reduction in the overall $Nd^{3+} \rightarrow Yb^{3+}$ energy-transfer efficiency.

### A. Singly doped crystals: Suitability for $Nd^{3+} \rightarrow Yb^{3+}$ resonant energy transfer

The unpolarized emission spectrum of SBN60:$Nd^{3+}$ together with the unpolarized absorption spectrum of SBN60:$Yb^{3+}$ in the 840–1040 nm spectral range are portrayed in Fig. 1. In this spectral region, where overlap exists, the emission spectrum of $Nd^{3+}$ corresponds to its $^4F_{3/2} \rightarrow {}^4I_{9/2}$ transition ($4f^3$ electronic configuration), while the absorption spectrum of $Yb^{3+}$ is related to its unique $^2F_{7/2} \rightarrow {}^2F_{5/2}$ transition ($4f^{13}$ electronic configuration). It should be noted that in contrast with the majority of crystals or glasses codoped with $Nd^{3+}$ and $Yb^{3+}$ ions,[10–14] a clear overlap in the spectral range of 880–940 nm exists between the $Nd^{3+}$-emission (donor) and $Yb^{3+}$-absorption (acceptor) spectra in SBN60. This unusual nonvanishing donor-acceptor overlap is due to the very broad optical bands of $Nd^{3+}$ and $Yb^{3+}$ ions in SBN60.[8,15] As previously described (Sec. III), such large inhomogeneous broadening is due to the large lattice site disorder. Moreover, for the particular case of SBN60:$Yb^{3+}$, the broadening is increased by the contribution of nonequivalent $Yb^{3+}$ centers,[9] together with a large homogeneous broadening due to the strong electron-phonon interaction typical of trivalent ytterbium ions in crystals.[16]

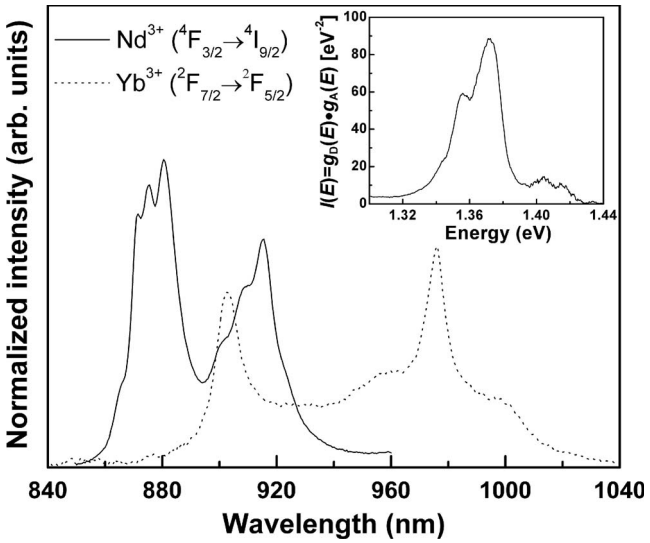


FIG. 1. Overlap region between $Nd^{3+}$ emission and $Yb^{3+}$ absorption (Ref. 15) in SBN. The inset shows the overlap function $I(E)=g_D(E)g_A(E)$.

At this point, it is important to mention that, according to the well-known Dexter model for resonant energy transfer,[17] the donor (D) to acceptor (A) transfer probability $W_{DA}$ is proportional to the overlap between the normalized donor emission line-shape function $g_D(E)$ and the normalized acceptor absorption line-shape function $g_A(E)$, i.e., $W_{DA} \propto \int g_D(E)g_A(E)dE$. The overlap function, $I(E)=g_D(E)g_A(E)$, has been displayed in the inset of Fig. 1, so that a value of 3.1 $eV^{-1}$ is obtained for the overlap integral, $\int I(E)dE$. This value is in contrast with those obtained for a variety of other Nd, Yb doubly doped crystals or glasses, for which a nonvanishing overlap integral is only obtained by means of a phonon-assisted mechanism.[10–14]

A schematic diagram of energy positions for the different $^{2S+1}L_J$ states of $Nd^{3+}$ and $Yb^{3+}$ ions for the particular case of SBN60 host crystal is portrayed in Fig. 2. This diagram was obtained from our absorption and luminescence data and

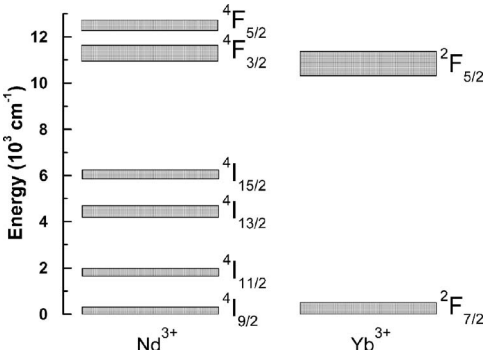


FIG. 2. Energy level diagram of $Nd^{3+}$ (donor) and $Yb^{3+}$ (acceptor) ions in SBN.

from those previously reported.[15] The $^4F_{3/2}$ ($Nd^{3+}$) and $^2F_{5/2}$ ($Yb^{3+}$) metastable excited states in SBN60 are much closer in energy [$\Delta E \approx 636$ cm$^{-1}$ (see Fig. 1)] than in a large variety of other hosts[10–14] (see Fig. 3), providing a nonvanishing matching between the optical spectra of $Yb^{3+}$ and $Nd^{3+}$ ions. This short energy gap represents an important aspect, as any thermal assistance is not necessary in order to have an efficient energy transfer. Nevertheless, a larger overlap integral (5.5 eV$^{-1}$) can still be achieved if the process is assisted by the 630 cm$^{-1}$ phonons (the most intense Raman mode of SBN60 at room temperature[18]). Thus, in spite of the second order nature of phonon-assisted energy transfer, the participation of this process could affect the net energy-transfer efficiency.

For the sake of comparison to other Nd, Yb doubly doped materials, Fig. 3 shows a plot of the nonphonon-assisted overlap integral of the $Nd^{3+}$-emission and $Yb^{3+}$-absorption normalized band shapes as a function of the energy gap $\Delta E$ between the $^4F_{3/2}$ ($Nd^{3+}$) and $^2F_{5/2}$ ($Yb^{3+}$) excited states for a

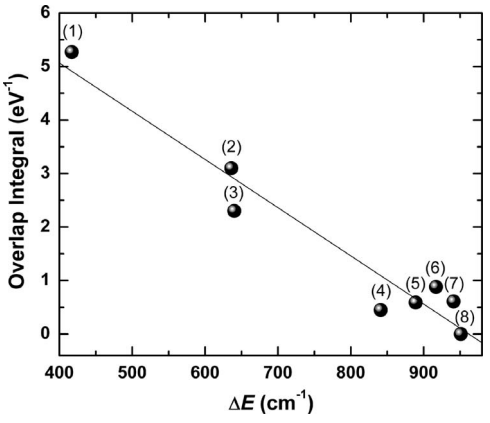


FIG. 3. Overlap integral of $Nd^{3+}$-emission and $Yb^{3+}$-absorption normalized band shapes versus energy gap between the $^4F_{3/2}$ ($Nd^{3+}$) and $^2F_{5/2}$ ($Yb^{3+}$) excited states for (1) $K_5Bi_{0.9-x}Nd_xYb_{0.1}(MoO_4)_4$ (Ref. 19), (2) SBN:Nd:Yb (this work), (3) $YAlO_3$:Nd:Yb (Ref. 20), (4) $Cs_2NaNd_{0.4}Yb_{0.6}Cl_6$ (Ref. 10), (5) $Pb(PO_3)_2$:Nd:Yb (Ref. 11), (6) $30PbF_2 \cdot 20GaF_3 \cdot 15InF_3 \cdot 15ZnF_2 \cdot (19-x)CaF_2 \cdot xYbF_3 \cdot 1NdF_3$ (Ref. 12), (7) $60ZrF_4 \cdot 30BaF_2 \cdot 4LaF_3 \cdot 1NdF_3 \cdot 5YbF_3$ (Ref. 13), and (8) $YAl_3(BO_3)_4$:Nd:Yb (Ref. 14).

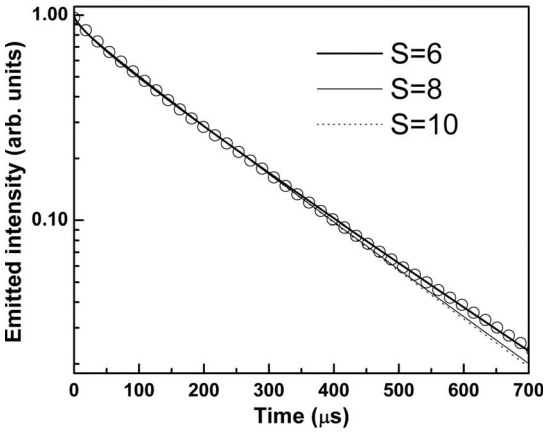


FIG. 4. Time dependence of $Nd^{3+}$ emission ($^4F_{3/2} \rightarrow {}^4I_{11/2}$) obtained for the crystal Nd1Yb5. Open circles are experimental data and solid lines are the best fit to expression (1) for dipole-dipole ($S=6$), dipole-quadrupole ($S=8$), and quadrupole-quadrupole ($S=10$) interactions.

variety of hosts.[10–14,19,20] $\Delta E$ was determined from the distance between the barycenters of the $^4F_{3/2} \rightarrow {}^4I_{9/2}$ ($Nd^{3+}$) emission and $^2F_{7/2} \rightarrow {}^2F_{5/2}$ ($Yb^{3+}$) absorption. A first inspection of Fig. 3 shows a general trend, the overlap increases linearly as the energy gap decreases. We can also appreciate that only a larger overlap than the one obtained in SBN60:Yb:Nd has been reported for the molibdate $K_5Bi_{0.9}Yb_{0.1}(MoO_4)_4$:Nd.[19] It should also be noted that compared to $YAlO_3$:Nd,[20] with almost the same energy gap, the overlap is higher in SBN60. This fact must be again attributed to the large inhomogeneous broadening in the optical bands of $Nd^{3+}$ and $Yb^{3+}$ ions in SBN60. Therefore, SBN60 can be considered an excellent host for an efficient $Nd^{3+} \rightarrow Yb^{3+}$ energy transfer.

### B. $Nd^{3+} \rightarrow Yb^{3+}$ energy-transfer mechanism

The shape of decay-time curves obtained under pulsed excitation is now analyzed to determine the mechanism responsible for the $Nd^{3+} \rightarrow Yb^{3+}$ energy transfer. By codoping the SBN60:$Nd^{3+}$ crystal with $Yb^{3+}$ ions, an increase is observed in the decay rate of the $Nd^{3+}$ ion emission, indicating that $Nd^{3+} \rightarrow Yb^{3+}$ energy transfer takes place via a nonradiative process.

The decay-time curves of the $Nd^{3+}$ emission from the metastable state $^4F_{3/2}$ in SBN60:$Nd^{3+}$:$Yb^{3+}$ display a nonexponential shape. As an example, Fig. 4 shows the $^4F_{3/2} \rightarrow {}^4I_{11/2}$ emission intensity (monitored at 1060 nm) versus decay time for the Nd1Yb5 crystal. According to previous models, considering a short-time excitation and the existence of energy migration among donors, this decay-time curve follows the expression[21,22]

$$I(t) = I_0 \exp\left[-\frac{t}{\tau_0} - \gamma_S t^{3/S} - wt\right], \quad (1)$$

where $t$ is the time after excitation, $\tau_0$ (=215 $\mu$s) (Ref. 8) is the intrinsic lifetime of $Nd^{3+}$ (donor ions), $\gamma_s$ (with $S=6$, 8, and 10 for dipole-dipole, dipole-quadrupole, and quadrupole-

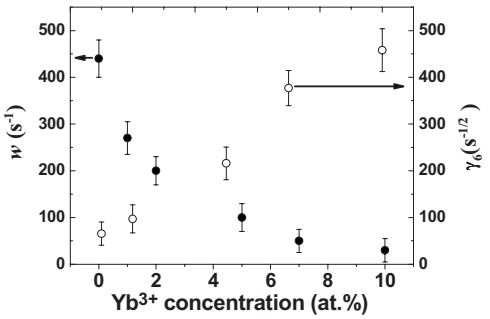


FIG. 5. Energy diffusion ($w$) and direct $Nd^{3+} \rightarrow Yb^{3+}$ energy-transfer ($\gamma_6$) parameters as a function of $Yb^{3+}$ content in SBN:$Nd^{3+}$:$Yb^{3+}$.

quadrupole interactions, respectively) is a time independent constant related to the direct $Nd^{3+} \rightarrow Yb^{3+}$ energy transfer (static transfer), and $w$ is the migration parameter (dynamic transfer), which takes into account the donor migration. The time dependence of the $^4F_{3/2} \rightarrow {}^4I_{11/2}$ luminescence of $Nd^{3+}$ ions excited at 808 nm ($^4F_{5/2}$ state) for the different samples was fitted to Eq. (1), assuming dipole-dipole ($S=6$), dipole-quadrupole ($S=8$), and quadrupole-quadrupole ($S=10$) couplings. The best agreement between experimental data and theoretical fit is achieved for $S=6$, as observed for the Nd1Yb5 sample (Fig. 4). Therefore, it can be inferred that an electric dipole-dipole interaction mechanism is dominant in the energy-transfer process. This type of interaction has been usually found in other $Nd^{3+}$-$Yb^{3+}$ codoped hosts.[12,14,19] For such interaction, $\gamma_6$ is given by[21]

$$\gamma_6 = \frac{4}{3}\pi^{3/2}\rho_A\sqrt{C_{DA}}, \tag{2}$$

where $\rho_A$ is the acceptor density and $C_{DA}$ is the so-called energy-transfer microparameter. This physical quantity is used to compare the ability of a given donor-acceptor system for energy transfer independently of the donor-acceptor distance. From the fitting of the decay curve in Fig. 4 to expression (1), a value of $21.6 \pm 0.1$ $s^{-1/2}$ is obtained for $\gamma_6$. Then, using Eq. (2), we can estimate the energy-transfer microparameter for the Nd1Yb5 sample. $C_{DA}$ resulted to be about $5.6 \times 10^{-40}$ $cm^6/s$ using an $Yb^{3+}$ ion concentration $\rho_A \approx 1.23 \times 10^{20}$ ions/$cm^3$. The value estimated for $\rho_A$ was taken to be equal to 15% of the content added to the melt, corresponding to the $Yb^{3+}$ average concentration measured by total x-ray fluorescence. In fact, the concentration of $Yb^{3+}$ segregated in the crystal ranged between 10% and 20% of that added to the melt for the different SBN60:$Yb^{3+}$:$Nd^{3+}$ samples here studied. The fitting of the decay curve in Fig. 4 to Eq. (1) leads to a migration transfer rate of $w = 100 \pm 4$ $s^{-1}$ for the Nd1Yb5 crystal.

Similar values for $C_{DA}$ were obtained for the samples doped with other $Yb^{3+}$ concentrations. On the contrary, the energy migration rate ($w$) and the direct $Nd^{3+} \rightarrow Yb^{3+}$ energy-transfer parameter ($\gamma_6$) display variations with the $Yb^{3+}$ content. As shown in Fig. 5, $w$ decreases from $440 \pm 2$ $s^{-1}$ (Nd1 sample) to $30 \pm 20$ $s^{-1}$ (Nd1Yb10 sample), whereas $\gamma_6$ increases from $6.5 \pm 0.1$ $s^{-1/2}$ (Nd1Yb1 sample) to $45.8 \pm 0.3$ $s^{-1/2}$ (Nd1Yb10 sample). Indeed, the results shown in Fig. 5 manifest a weak contribution of donor energy migration (when compared to $1/\tau_0$), which gradually decreases with the Yb (acceptor) content.

The value obtained for the energy-transfer microparameter in SBN60 ($\sim 5.8 \times 10^{-40}$ $cm^6/s$) is lower than that reported for molybdate crystals ($13.4 \times 10^{-40}$ $cm^6/s$),[19] but higher than the one found in fluoroindogallate glasses ($3.2 \times 10^{-40}$ $cm^6/s$).[12] This seems to be in relatively good agreement with the results given in Fig. 3: The larger overlap between the optical bands of $Nd^{3+}$ and $Yb^{3+}$ ions, the higher energy-transfer microparameter. However, this trend does not hold when comparing to yttrium aluminium borate (YAB) crystals,[14] as for this crystal host, a much larger energy-transfer microparameter ($180.0 \times 10^{-40}$ $cm^6/s$) has been reported, while having a vanishing resonant overlap between the optical bands of $Nd^{3+}$ and $Yb^{3+}$ ions. Anyhow, for this crystal, a large one phonon-assisted overlap (13.7 $eV^{-1}$ with a phonon energy of about 1030 $cm^{-1}$) has been reported at room temperature.[14]

It seems to be that those materials with high energy effective phonons bridging $\Delta E$ (energy separation between the excited states of $Nd^{3+}$ and $Yb^{3+}$ ions) present very high microparameters that cannot be explained in terms of the trend observed in Fig. 3. However, this not applies to low energy effective phonon materials, as, for example, SBN. For this crystal, $\Delta E$ (636 $cm^{-1}$) matches the energy of the effective phonons (630 $cm^{-1}$). In spite of this excellent matching, the microparameter behaves as expected from Fig. 3, i.e., dominated by the resonant energy-transfer term. In fact, it has been previously reported that the phonon-assisted $Nd^{3+} \rightarrow Yb^{3+}$ energy transfer is less important for low energy gap materials than for high energy gap materials.[12] Thus, for YAB, where high energy effective phonons of 1030 $cm^{-1}$ bridge the energy separation $\Delta E$, a much higher microparameter than that expected from the trend of Fig. 3 is observed. Therefore, for those cases, Fig. 3 would not be useful to predict the microparameter tendency.

### C. Influence of $Yb^{3+}$ concentration on the energy-transfer efficiency

In this section, we analyze the emission spectra as well the decay-time curves of $Nd^{3+}$ (donor) and $Yb^{3+}$ (acceptor) for the doubly doped samples, so that the effect of $Yb^{3+}$ content on the $Nd^{3+} \rightarrow Yb^{3+}$ energy-transfer efficiency can be determined.

Figure 6 shows the emission spectra obtained for all the $Yb^{3+}$ concentrations used in the present work. They consist of broad emission bands corresponding to the $Nd^{3+}$ ($^4F_{3/2} \rightarrow {}^4I_{9/2}$ and $^4F_{3/2} \rightarrow {}^4I_{11/2}$) and $Yb^{3+}$ ($^2F_{5/2} \rightarrow {}^2F_{7/2}$) emissions. All these spectra were normalized to the $^4F_{3/2} \rightarrow {}^4I_{9/2}$ emission spectrum of $Nd^{3+}$ ions, as it is well isolated from the $Yb^{3+}$ spectrum. The excitation wavelength was carried out through the $Nd^{3+}$ ion $^4I_{9/2} \rightarrow {}^4F_{5/2}$ transition at 808 nm. It can be appreciated that the $Yb^{3+}$-emission intensity (obtained via $Nd^{3+}$ excitation) increases with the concentration of acceptor ions, which evidences an increase in the $Nd^{3+} \rightarrow Yb^{3+}$ energy-transfer efficiency.

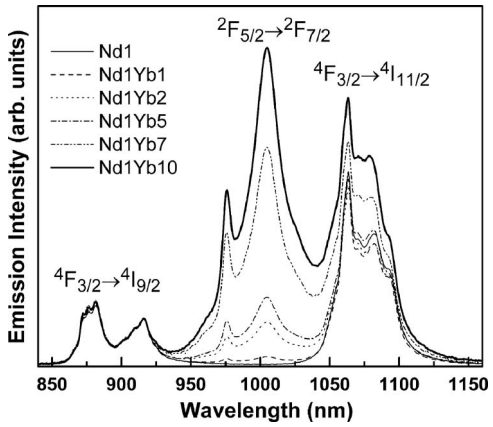


FIG. 6. Emission spectra of the different SBN:Nd:Yb crystals obtained by exciting the $Nd^{3+}$ ions (at 808 nm).

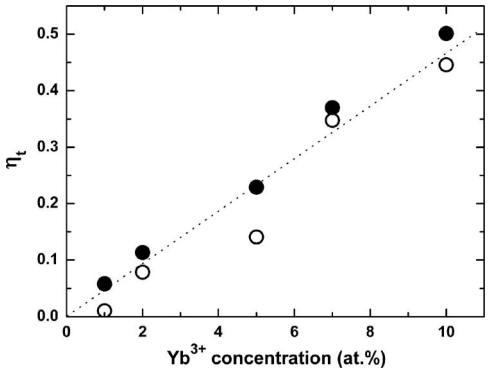


FIG. 7. $Nd^{3+} \rightarrow Yb^{3+}$ energy-transfer efficiency as a function of $Yb^{3+}$ content obtained from spectral data (Fig. 6) and Eq. (4) (white dots) and from decay data (Fig. 9) and Eq. (5) (black dots). The dotted line is drawn to guide the eyes.

From the emission spectra shown in Fig. 6, the energy-transfer efficiency can be determined as a function of the $Yb^{3+}$ concentration. In a first order approximation, the room temperature $Nd^{3+} \leftarrow Yb^{3+}$ back transfer can be considered negligible in comparison to the $Nd^{3+} \rightarrow Yb^{3+}$ direct energy transfer. Thus, the energy-transfer efficiency $\eta_t$ (defined as the number of $Nd^{3+}$ ions deexcited per unit time via $Yb^{3+}$ ions divided by the total number of $Nd^{3+}$ ions deexcited per unit of time in steady conditions) is given by[14]

$$\eta_t = \frac{n^e_{\mathrm{Nd}} W_t n^o_{\mathrm{Yb}}}{n^e_{\mathrm{Nd}}(W^r_{\mathrm{Nd}} + W^{\mathrm{nr}}_{\mathrm{Nd}}) + n^e_{\mathrm{Nd}} W_t n^o_{\mathrm{Yb}}}, \tag{3}$$

where $n^e_{\mathrm{Nd}} W_t n^o_{\mathrm{Yb}}$ gives the density of $Nd^{3+}$ ions deexcited via $Yb^{3+}$ ions per unit of time, $W_t$ being the so-called $Nd^{3+} \rightarrow Yb^{3+}$ energy-transfer term, and $n^e_{\mathrm{Nd}}$ and $n^o_{\mathrm{Yb}}$ the population densities of $Nd^{3+}$ ions in its $^4F_{3/2}$ excited state and $Yb^{3+}$ ions in its $^2F_{7/2}$ ground state, respectively (see Fig. 2). It should be noted that, in this notation, the product $W_t n^o_{\mathrm{Yb}}$ gives the energy-transfer rate. The term $n^e_{\mathrm{Nd}}(W^r_{\mathrm{Nd}} + W^{\mathrm{nr}}_{\mathrm{Nd}})$ gives the density of $Nd^{3+}$ ions that are deexcited per unit of time in the absence of energy transfer and $W^r_{\mathrm{Nd}}$ and $W^{\mathrm{nr}}_{\mathrm{Nd}}$ being the radiative and nonradiative decay probabilities from the $^4F_{3/2}$ state of $Nd^{3+}$ ions, respectively. From previous works[11,14] it has been shown that $\eta_t$ in Eq. (3) can be expressed in terms of spectral data and intrinsic fluorescence quantum efficiencies of both $Nd^{3+}$ ($\eta_{\mathrm{Nd}}$) and $Yb^{3+}$ ($\eta_{\mathrm{Yb}}$),

$$\eta_t \approx \frac{\dfrac{1}{\eta_{\mathrm{Yb}}} \displaystyle\int_{850\ \mathrm{nm}}^{1150\ \mathrm{nm}} I_{\mathrm{Yb}}(\lambda) d\lambda}{\left(1 + \dfrac{\beta^4_{I_{13/2}} + \beta^4_{I_{15/2}}}{\beta^4_{I_{9/2}} + \beta^4_{I_{11/2}}}\right) \dfrac{1}{\eta_{\mathrm{Nd}}} \displaystyle\int_{850\ \mathrm{nm}}^{1150\ \mathrm{nm}} I_{\mathrm{Nd}}(\lambda) d\lambda + \dfrac{1}{\eta_{\mathrm{Yb}}} \displaystyle\int_{850\ \mathrm{nm}}^{1150\ \mathrm{nm}} I_{\mathrm{Yb}}(\lambda) d\lambda}, \tag{4}$$

where $I(\lambda)$ represents the spectral luminescence intensity, and $\beta^4_{I_{9/2}}$, $\beta^4_{I_{11/2}}$, $\beta^4_{I_{13/2}}$, and $\beta^4_{I_{15/2}}$ are the branching ratios of the four transitions from the $^4F_{3/2}$ metastable state to the $^4I_J$ multiplets of $Nd^{3+}$. From the ratio between the $^4F_{3/2}$ state fluorescence lifetime measured for our Nd1 sample (198 $\mu$s) and the radiative lifetime previously reported (257 $\mu$s),[8] we obtain $\eta_{\mathrm{Nd}} \approx 0.8$. This value is close to that (0.84) obtained from a SBN60 crystal doped with 0.4 at. % of $Nd^{3+}$ ions (as determined by x-ray fluorescence measurements).[8] The $Yb^{3+}$ multiphonon relaxation rate is expected to be negligible because the energy gap between the two ($^2F_{5/2}$ excited and $^2F_{7/2}$ ground) involved states (about 9800 $cm^{-1}$) requires near to 16 630 $cm^{-1}$ phonons to be bridged. Thus, the radiative lifetime of $Yb^{3+}$ luminescence can be considered as its fluorescence lifetime at low temperature (10 K), and hence, the quantum efficiency at room temperature was estimated to be $\eta_{\mathrm{Yb}} \approx 0.9$ [$Yb^{3+}$ ion fluorescence lifetime at room temperature ($\tau_F$) divided by that at 10 K ($\tau_{\mathrm{rad}}$) reported for a SBN60:$Yb^{3+}$ (0.34 at. %) crystal[15]].

Now, the $Nd^{3+} \rightarrow Yb^{3+}$ energy-transfer efficiency $\eta_t$ as a function of the $Yb^{3+}$ acceptor ion concentration can be estimated from our emission spectra (Fig. 6) and Eq. (4) using the branching ratios previously reported for the $Nd^{3+}$ in SBN60 ($\beta^4_{I_{9/2}} = 0.396$, $\beta^4_{I_{11/2}} = 0.5$, $\beta^4_{I_{13/2}} = 0.1$, and $\beta^4_{I_{15/2}} = 0.004$),[23] $\eta_{\mathrm{Nd}} \approx 0.8$ and $\eta_{\mathrm{Yb}} \approx 0.9$. This dependence is displayed in Fig. 7. We see that the net transfer efficiency increases linearly with the $Yb^{3+}$ ion concentration up to close to 50% for a 10 at. % of $Yb^{3+}$ concentration. Moreover, it is important to note that the transfer efficiency does not saturate in this $Yb^{3+}$ concentration range. This result suggests that an

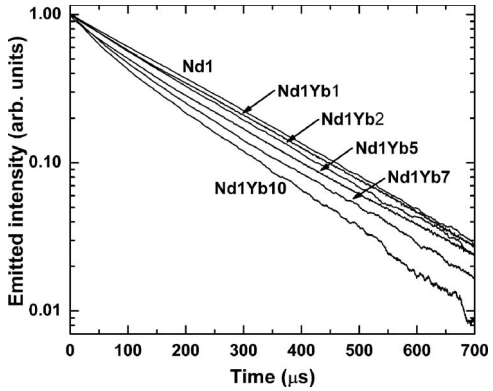


FIG. 8. Time evolution of the $Nd^{3+}$ emission ($^4F_{3/2} \rightarrow {}^4I_{11/2}$) obtained for the samples Nd1, Nd1Yb1, Nd1Yb2, Nd1Yb5, Nd1Yb7, and Nd1Yb10 excited at 808 nm.

additional increase in the $Yb^{3+}$ content would lead to a further increase in the net transfer efficiency.

The transfer efficiency $\eta_t$ can also be obtained from decay-time data. In this case, it is given by

$$\eta_t = 1 - \frac{\tau_{\text{Nd-Yb}}}{\tau_{\text{Nd}}}, \tag{5}$$

where $\tau_{\text{Nd-Yb}}$ and $\tau_{\text{Nd}}$ are the $Nd^{3+}$ luminescence lifetimes of the $^4F_{3/2}$ excited state in the presence and absence of $Yb^{3+}$ ions, respectively. The time evolution of the $Nd^{3+}$ emission from the $^4F_{3/2}$ state (monitored at 1060 nm) for the Nd1, Nd1Yb1, Nd1Yb2, Nd1Yb5, Nd1Yb7, and Nd1Yb10 samples is portrayed in Fig. 8. In the doubly doped samples, the $Nd^{3+}$ luminescence decay-time curves have no exponential shape, so that the lifetime was taken as the time at which the luminescence intensity has decayed to $e^{-1}$ of its initial value. From Fig. 8, it can also be seen that the $Nd^{3+}$ luminescence decays faster as the $Yb^{3+}$ concentration is increased. The dependence of $\tau_{\text{Nd-Yb}}$ on the $Yb^{3+}$ concentration is shown in Fig. 9, from which a significant reduction of the $Nd^{3+}$-emission lifetime by increasing the $Yb^{3+}$ concentration can be appreciated. Now, the $Nd^{3+} \rightarrow Yb^{3+}$ energy-transfer

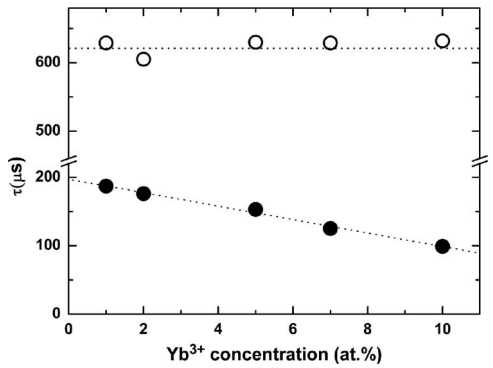


FIG. 9. Lifetimes of $Nd^{3+}$ luminescence (excited at 808 nm; black dots) and $Yb^{3+}$ luminescence (excited at 903 nm; white dots) as a function of $Yb^{3+}$ content in SBN:$Nd^{3+}$:$Yb^{3+}$. Dotted lines are drawn to guide the eyes.

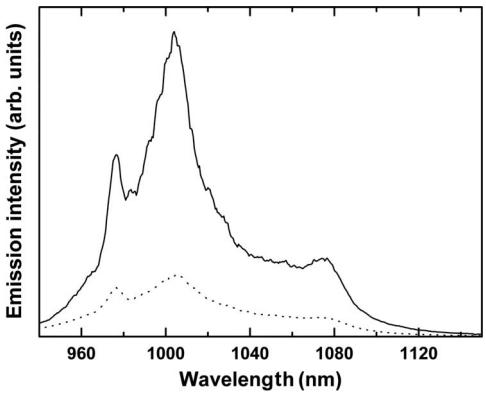


FIG. 10. Room temperature emission spectra obtained from the Nd1Yb10 sample under 920 nm ($Yb^{3+}$) excitation. Excitation intensity was 5 kW/cm$^2$ (dashed line) and 25 kW/cm$^2$ (solid line).

efficiency can be obtained as a function of $Yb^{3+}$ concentration using Eq. (5), the decay-time data ($\tau_{\text{Nd-Yb}}$) displayed in Fig. 9, and the $Nd^{3+}$ luminescence decay time ($\tau_{\text{Nd}} = 198\ \mu$s) obtained for the $Nd^{3+}$ singly doped crystal (Nd1 sample). The transfer efficiencies obtained in such a way have been displayed in Fig. 7 for the sake of comparison with those obtained from continuous wave emission spectra. This figure shows a good agreement between energy-transfer efficiencies obtained from emission spectra and those obtained from decay-time measurements. This fact indicates that radiative energy-transfer contribution to the total $Nd^{3+} \rightarrow Yb^{3+}$ energy transfer can be considered negligible, since a radiative energy transfer does not cause any reduction in donor lifetime.[24]

### D. $Nd^{3+} \leftarrow Yb^{3+}$ back energy transfer

In this section, we have investigated the presence of $Nd^{3+} \leftarrow Yb^{3+}$ back transfer processes in SBN60 crystals, as it could lead to a reduction in the overall $Nd^{3+} \rightarrow Yb^{3+}$ energy-transfer efficiency. In fact, this reduction could lead to deterioration in the laser performance of the $Nd^{3+}$, $Yb^{3+}$ codoped SBN60 crystals operating under $Nd^{3+}$ excitation. Two main cross relaxation mechanisms could give place to the activation of $Nd^{3+} \leftarrow Yb^{3+}$ back transfer processes. These mechanisms are (a) $Yb(^2F_{5/2})$, $Nd(^4I_{9/2}) \rightarrow Yb(^2F_{7/2})$, $Nd(^4F_{3/2})$ cross relaxation (see Fig. 2) and (b) $Yb(^2F_{5/2})$, $Nd(^4F_{3/2}) \rightarrow Yb(^2F_{7/2})$, $Nd(^4G)$ cross relaxation. The $^4G$ states (not displayed in Fig. 2) are positioned at higher energies than the $^4F_{5/2}$ state. The possible existence of both processes and their corresponding influence on the overall $Nd^{3+} \rightarrow Yb^{3+}$ energy-transfer efficiency is analyzed next.

(a) $Yb(^2F_{5/2})$, $Nd(^4I_{9/2}) \rightarrow Yb(^2F_{7/2})$, $Nd(^4F_{3/2})$ cross relaxation. The possible presence of this mechanism has been investigated by only exciting the $Yb^{3+}$ ions. In Fig. 10, we show the emission spectra obtained for the Nd1Yb10 sample under 920 nm ($Yb^{3+}$) excitation for two pump excitation intensities: 5 and 25 kW/cm$^2$ (maximum excitation intensity achieved in our laboratory at 920 nm). Only the broad emission band characteristic of $Yb^{3+}$ ions is observed without any contribution from $Nd^{3+}$ ions. Consequently, the presence of

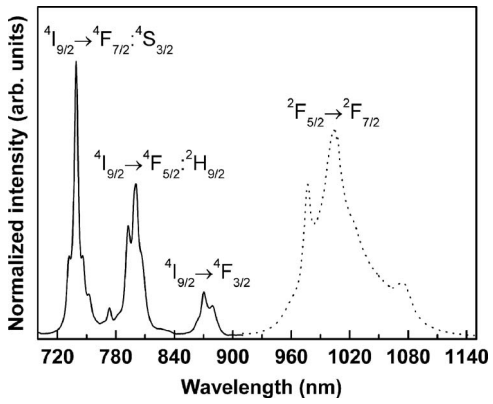


FIG. 11. $Nd^{3+}$-absorption spectrum (solid line) and $Yb^{3+}$-emission spectrum (dashed line) in SBN60.

$Nd^{3+} \leftarrow Yb^{3+}$ back transfer by means of $Yb^{3+}(^2F_{5/2})$, $Nd^{3+}(^4I_{9/2}) \rightarrow Yb(^2F_{7/2})$, $Nd(^4F_{3/2})$ cross relaxation can be neglected, at least for the excitation intensities available in our experimental conditions. This conclusion is in agreement with the vanishing overlap between the $Yb^{3+}$ emission and $Nd^{3+}$ absorption, as shown in Fig. 11.

(b) $Yb(^2F_{5/2})$, $Nd(^4F_{3/2}) \rightarrow Yb(^2F_{7/2})$, $Nd(^4G)$ cross relaxation. Under $Nd^{3+}$ pumping, and due to the limited $Nd^{3+} \rightarrow Yb^{3+}$ energy-transfer efficiency, the metastable excited states of both $Nd^{3+}$ and $Yb^{3+}$ ions have a non-negligible population. Thus, one $Yb^{3+}$ excited ion could transfer its energy to one excited $Nd^{3+}$ ion, in such a way that this ion would be excited to its higher $^4G$ energy state. The net effect of this process would be a reduction in the excited-state population of $Yb^{3+}$ ions, i.e., a reduction in the overall $Nd^{3+} \rightarrow Yb^{3+}$ energy-transfer efficiency. Indeed, it is expected that this process would be highly dependent on the excitation intensity. Thus, in order to detect the presence of $Yb(^2F_{5/2})$, $Nd(^4F_{3/2}) \rightarrow Yb(^2F_{7/2})$, $Nd(^4G)$ cross relaxation assisted $Nd^{3+} \leftarrow Yb^{3+}$ back energy transfer, we have recorded the emission spectra after 808 nm ($Nd^{3+}$) excitation for different excitation intensities, ranging from 7 up to 36 $kW/cm^2$ (typical excitation intensities achieved in end-pumped SBN lasers). The obtained results are shown in Fig. 12. Note that the spectra in Fig. 12 have been normalized to the 890 nm emission peak. From the data displayed in this figure, we have calculated the $Nd^{3+} \rightarrow Yb^{3+}$ energy-transfer efficiency as a function of the excitation intensity by using Eq. (4). Results are displayed in the inset of Fig. 12. A small reduction (from 47% down to 43%) in the $Nd^{3+} \rightarrow Yb^{3+}$ energy-transfer efficiency has been obtained when the excitation intensity was increased from 7 up to 36 $kW/cm^2$. This reduction can be related to $Yb(^2F_{5/2})$, $Nd(^4F_{3/2}) \rightarrow Yb(^2F_{7/2})$, $Nd(^4G)$ cross relaxation processes. Nevertheless, the presence of such processes would lead to the population of the $Nd(^4G)$ states and, therefore, to the appearance of visible emissions from these states. This is not our case. Even for the highest excitation intensities, visible emissions were not detected. We state at this point that other mechanism different from $Yb(^2F_{5/2})$, $Nd(^4F_{3/2}) \rightarrow Yb(^2F_{7/2})$, $Nd(^4G)$ cross relaxation processes could be the origin of the reduction in the net energy-transfer efficiency. For example,

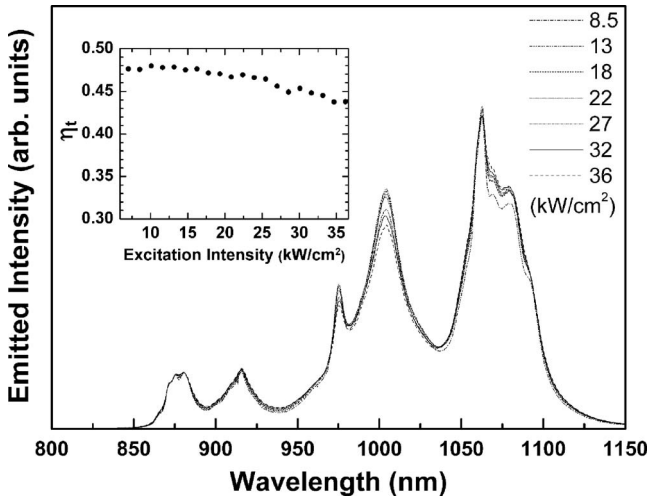


FIG. 12. Room temperature emission spectra obtained from the Nd1Yb10 sample excited at 808 nm for different excitation intensities. The inset shows the $Nd^{3+} \rightarrow Yb^{3+}$ energy-transfer efficiency as a function of the excitation intensity.

as it has been already demonstrated in other $Nd^{3+}$ and $Yb^{3+}$ codoped crystals,[25] pump induced thermal loading could lead to an increment in the phonon-assisted $Nd^{3+} \leftarrow Yb^{3+}$ back energy-transfer efficiency and therefore to a reduction in the net $Nd^{3+} \rightarrow Yb^{3+}$ energy-transfer efficiency.

According to the data displayed in Figs. 10 and 12, it is possible to state that the presence of $Nd^{3+} \leftarrow Yb^{3+}$ back energy transfer is negligible in steady state conditions, at least at room temperature and for moderate excitation intensities. In order to confirm this statement, we have also monitored the time decay curve of $Yb^{3+}$ emission after both $Nd^{3+}$ and $Yb^{3+}$ excitations. The decay-time curve of the $Yb^{3+}$ emission, obtained under $Nd^{3+}$ excitation (at 808 nm), exhibits an initial rise at a rate in accordance to excitation via energy transfer from $Nd^{3+}$ ions. After this initial rise, related to the $^4F_{3/2}$ ($Nd^{3+}$) fluorescence lifetime, the $Yb^{3+}$ luminescence presents an exponential decay time. This decay time corresponds to that obtained for direct excitation of $Yb^{3+}$ ions in SBN60:Yb:Nd crystals, and it essentially coincides with that obtained for singly doped SBN60:Yb crystals. As an example, Fig. 13(a) shows the $Yb^{3+}$ luminescence decay-time curve (monitored at 1004 nm) obtained for the Nd1Yb5 sample, when exciting into $Nd^{3+}$ ions (808 nm). For this Yb concentration, the decay-time curve shows a rise time of about 150 $\mu$s followed by an exponential decay with a lifetime of about 630 $\mu$s. This value is essentially that obtained for a SBN:Yb crystal, with the same $Yb^{3+}$ content (Yb5) [see Fig. 13(b)]. Furthermore, the decay time obtained for the $Yb^{3+}$ emission was found to be independent of the ytterbium content, and it is not affected by the presence of $Nd^{3+}$ ions (see Fig. 9), indicating a negligible $Nd^{3+} \leftarrow Yb^{3+}$ energy transfer. This conclusion obtained from the analysis of the decay curves is found to be in accordance with experimental data included in Figs. 10–12.

## V. CONCLUSIONS

Resonant $Nd^{3+} \rightarrow Yb^{3+}$ energy transfer takes place in $Nd^{3+}$ and $Yb^{3+}$ ion codoped $Sr_{0.6}Ba_{0.4}(NbO_3)_2$ crystals because of

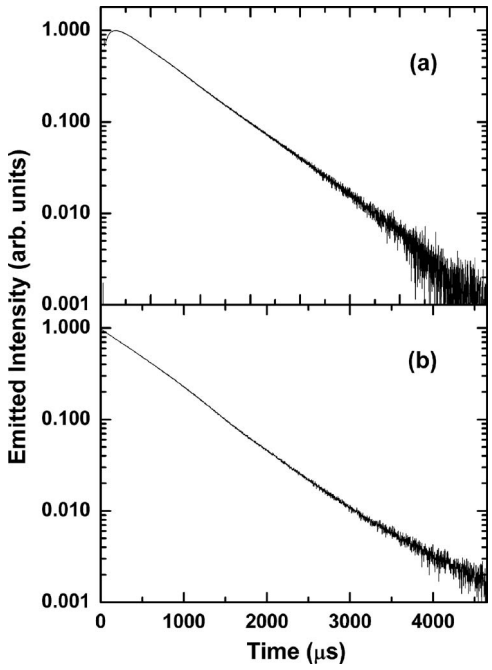


FIG. 13. Time evolution of $Yb^{3+}$ emission (1004 nm) obtained for (a) the Nd1Yb5 crystal (excited at 808 nm) and (b) the Yb5 crystal (excited at 903 nm).

the very broad optical bands of $Nd^{3+}$ ($^4F_{3/2} \rightarrow {}^4I_{9/2}$ emission) and $Yb^{3+}$ ($^2F_{7/2} \rightarrow {}^2F_{5/2}$ absorption) ions, giving rise to a significant spectral overlap. This fact is in contrast with the vanishing overlap usually observed for many other $Nd^{3+}-Yb^{3+}$ codoped hosts.[10–14] The $Nd^{3+} \rightarrow Yb^{3+}$ energy transfer mainly occurs via a nonradiative process. In fact, the good agreement between energy-transfer efficiencies obtained from emission spectra and decay-time data indicates a negligible contribution of radiative energy transfer to the net $Nd^{3+} \rightarrow Yb^{3+}$ energy-transfer process. Analysis of Nd-emission decay-time curves revealed that an electric dipole-dipole interaction mechanism is dominant in the energy-transfer process. Back transfer has not been observed at room temperature and moderate excitation intensities (those used in end-pumped lasers) within the investigated $Yb^{3+}$ concentration range. The transfer efficiency is enhanced by increasing the acceptor concentration, being about 50% for the most $Yb^{3+}$ concentrated crystal (10 at. %). Such efficiency does not saturate and therefore an increase in the $Yb^{3+}$ content could lead to a further increase in the transfer efficiency.

The high energy-transfer efficiency achieved with the Nd1Yb10 sample suggests that codoping SBN60:$Yb^{3+}$ crystals with $Nd^{3+}$ ions (with multiple pump channels) could eventually provide additional pumping channels. This good versatility, combined with the exceptional laser and nonlinear properties of SBN60, indicates that the SBN60:$Nd^{3+}$:$Yb^{3+}$ optical material shows a great potential to develop diode pumped laser sources tunable in the visible region by different self-frequency sum mixing processes involving pump and laser radiations.

## ACKNOWLEDGMENTS

This work has been supported by the Spanish Ministry of Science and Technology under Contract No. MAT2004-03347 and by the CONACyT (México) under Contract No. 43016-F. One of us, U. Caldiño, wishes to thank the Spanish Ministry of Science and Education for a sabbatical stay financial support (Ref. No. SAB2004-0002).

*On leave from Departamento de Física, UAM, Iztapalapa, P.O. Box 55-534, 09340 México Distrito Federal, México.

[1] E. Montoya, J. Capmany, L. E. Bausá, T. Kellner, A. Diening, and G. Huber, Appl. Phys. Lett. **74**, 3113 (1999).
[2] J. J. Romero, D. Jaque, J. García-Solé, and A. A. Kaminskii, Appl. Phys. Lett. **78**, 1961 (2001).
[3] V. Petit, P. Camy, J. L. Doualan, and R. Moncorge, Appl. Phys. Lett. **88**, 051111 (2006).
[4] P. V. Lenzo, E. G. Spencer, and A. A. Ballman, Appl. Phys. Lett. **11**, 23 (1967).
[5] J. J. Romero, D. Jaque, J. García-Solé, and A. A. Kaminskii, Appl. Phys. Lett. **81**, 4106 (2002).
[6] P. W. Whipps, J. Solid State Chem. **4**, 281 (1972).
[7] P. B. Jamieson, S. C. Abrahams, and J. L. Bernstein, J. Chem. Phys. **48**, 5048 (1968).
[8] J. J. Romero, D. Jaque, L. E. Bausá, A. A. Kaminskii, and J. García Solé, J. Lumin. **87-89**, 877 (2000).
[9] M. O. Ramírez, L. E. Bausá, A. Speghini, M. Bettinelli, L. Ivleva, and J. García Solé, Phys. Rev. B **73**, 035119 (2006).
[10] W. Ryba-Romanowski and S. Golab, J. Mol. Struct. **450**, 223 (1998).
[11] F. Liégard, J. L. Doualan, R. Moncorgé, and M. Bettinelli, Appl. Phys. B: Lasers Opt. **80**, 985 (2005).
[12] F. Batalioto, D. F. de Sousa, M. J. V. Bell, R. Lebullenger, A. C. Hernandes, and L. A. O. Nunes, J. Non-Cryst. Solids **273**, 233 (2000).
[13] J. Qiu, M. Shojiya, R. Kanno, and Y. Kawamoto, Opt. Mater. (Amsterdam, Neth.) **13**, 319 (1999).
[14] D. Jaque, M. O. Ramírez, L. E. Bausá, J. García-Solé, E. Cavalli, A. Speghini, and M. Bettinelli, Phys. Rev. B **68**, 035118 (2003).
[15] M. O. Ramírez, D. Jaque, L. Ivleva, and L. E. Bausá, J. Appl. Phys. **95**, 6185 (2004).
[16] A. Lupei, V. Lupei, C. Presura, V. N. Enaki, and A. Petraru, J. Phys.: Condens. Matter **11**, 3769 (1999).
[17] D. L. Dexter, J. Chem. Phys. **21**, 836 (1953).
[18] A. Speghini, M. Bettinelli, U. Caldiño, M. O. Ramírez, D. Jaque, L. E. Bausá, and J. García Solé, J. Phys. D **39**, 4930 (2006).
[19] R. Balda, J. Fernández, I. Iparraguirre, and M. Al-Saleh, Opt. Mater. (Amsterdam, Neth.) **28**, 1247 (2006).
[20] M. J. Weber, Phys. Rev. B **4**, 3153 (1971).
[21] A. I. Burshtein, Sov. Phys. JETP **35**, 882 (1972).
[22] T. Förster, Z. Naturforsch. A **4A**, 321 (1949).
[23] J. J. Romero, Ph.D thesis, Universidad Autónoma de Madrid, 2002.
[24] B. Henderson and G. F. Imbusch, *Optical Spectroscopy of Inorganic Solids* (Clarendon, Oxford, 1989).
[25] D. Jaque, J. García-Solé, L. Macalik, J. Hanuza, and A. Majchrowski, Appl. Phys. Lett. **86**, 011920 (2005).